Int. J. Electrochem. Sci., 17 **(2022)** Article Number: 220627, doi: 10.20964/2022.06.43

International Journal of ELECTROCHEMICAL SCIENCE
www.electrochemsci.org

Synthesis and Characterization of Polyetheramine-type Benzoxazines as Protective Coatings for Low Carbon Steel against Corrosion in Sodium Chloride Solution

Chunxia Zhao[1,3,*], *Jixuan Wei*[1], *Jiaojiao Wu*[1], *Yuntao Li*[1,2,*], *Dong Xiang*[1], *Yuanpeng Wu*[1,3,4], *Hui Li*[1,3], *Zhaorun Hou*[1]

[1]School of New Energy and Materials, Southwest Petroleum University, Chengdu 610500, Sichuan, China
[2]State Key Laboratory Oil and Gas Reservoir Geology and Exploitation, Southwest Petroleum University, Chengdu 610500, Sichuan, China
[3] Sichuan Engineering Technology Research Center of Basalt Fiber Composites Development and Application
[4]The Center of Functional Materials for Working Fluids of Oil and Gas Field, Southwest Petroleum University, Chengdu 610500, Sichuan, China
Jixuan Wei and Jiaojiao Wu contributed equally to this work.
[*]E-mail: polychem@swpu.edu.cn (C. Z.), yuntaoli@swpu.edu.cn (Y. L.)

Received: 2 February 2022 / *Accepted:* 3 April 2022 / *Published:* 7 May 2022

Herein, based on the characteristics of flexible molecular structure design, polyetheramine benzoxazines with different molecular weights were prepared using solution synthesis, and their chemical structure was confirmed by Fourier transform infrared (FTIR) and proton nuclear magnetic resonance spectra. Three types of polybenzoxazine coatings were prepared on the surface of low carbon steel by coating and thermal curing methods. The FTIR analysis revealed the structural changes of benzoxazine coatings during curing, confirming the complete reaction of polybenzoxaine resin after heat curing. The surface morphology of the coatings was observed by scanning electron microscope. The coatings presented a continuous and uniform microstructure on the surface of low carbon steel, which overcomes the shortcomings of poor ductility and brittleness of traditional polybenzoxazine resins. In addition, the corrosion resistance of the coating was analyzed using electrochemical characterization. The results revealed that the corrosion current values of the polybenzoxazine coatings decreased by about two orders of magnitude compared to the pristine carbon steel. Moreover, the corrosion protection efficiency of the polybenzoxazine coatings was >98%, indicating promising application prospects of the blended coatings.

Keywords: polyetheramine; benzoxazine; anti-corrosive coating; corrosion performance

1. INTRODUCTION

Metals are extensively employed in the shipping, manufacturing, and construction industries due to their unique properties[1-2]. However, metals are easily corroded during operations, compromising their service life, wasting resources, and raising potential risks such as fire, explosion and other catastrophic accidents[3]. Statistically, the losses caused by metallic corrosion are increasing every year, indicating the urgent need for further research on corrosion prevention technologies for metals. One of the most widely used methods to reduce the corrosion rate is the utilization of polymeric coatings, which provide a physical barrier against corrosive media and reduce the corrosion rate[4-6]. At present, several polymers are used to prepare anti-corrosion coatings, including epoxy resin[7,8], polyaniline[9], and phenolic resin[10]. Among these polymers, phenolic resin is a promising coating material and adhesive due to its excellent properties, such as chemical resistance, adhesion and mechanical properties.

In recent years, polybenzoxazine (PBa) resin has been used as an anti-corrosion coating on the surface of low carbon steel due to its advantageous features, such as low surface energy[11,12], low water absorption, and extremely long shelf life. During the cross-linking polymerization of benzoxazine (Ba) monomer, small molecule by-products are not formed and the volumetric shrinkage rate is extremely low. Therefore, PBa-based coatings or films do not possess large areas of wrinkles and damages in the cured product, rendering good film-forming properties. As a stable barrier, PBa can isolate the metal from corrosive environment and prevent the ionic transmission and conduction of the corrosion reaction. Therefore, PBa resin is highly promising for preparing anti-corrosion coatings of metals[13-16]. In anti-corrosion coatings, PBa forms a stable network structure due to ring-opening polymerization, reducing the permeability of corrosive medium to the metal matrix and enhancing metallic life[17,18-20]. Lu et al.[21] synthesized benzoxazine (BA-a) with bisphenol A, aniline and paraformaldehyde as raw materials, and prepared a hydrophobic coating on the surface of mild steel by dipping coating and thermal curing methods, rendering excellent electrochemical properties. Their results showed that the corrosion resistance of PBA-a coating was improved with the increase in concentration of BA-a. For the sample with BA-a concentration of 500 g L^{-1}, when the curing temperature was increased from 150 °C to 210 °C, the protection efficiency of the PBA-a coating exceeded 99.0% and the anti-corrosion performance became better than that of epoxy resin. Huang et al.[22] prepared a cardanol-based PBa superhydrophobic coating on the surface of low-carbon steel by spraying and thermal curing. The hydrophobic coating presented excellent self-cleaning performance and thermal stability. When immersed in 3.5 wt% NaCl aqueous solution for 10 days, the coating also exhibited high corrosion resistance. Zhang et al.[23] prepared a bio-based Ba and mixed it with two other bio-based Ba monomers to prepare a series of copolymers. Their results revealed that these copolymers exhibited a synergistic effect to obtain low media electric constant, high cross-linking density, low corrosion current and high protection efficiency. However, most of the Ba monomers are solid powders, which do not easily form the desired coatings. When liquid Ba monomers are used to obtain thin films or coatings, the control over thickness and shape is increased, which expands their application areas, such as aerospace, electronics, automobile manufacturing, etc.

Inspired by the previous work, 4-(phenylazo)phenol, polyetheramine (D230, D400, D2000), and paraformaldehyde were used as reactants to synthesize three kinds of polyetheramine-type liquid benzoxazine monomers (Bza-d230, Bza-d400, Bza-d2000) in this study. These polyetheramine-type benzoxazines were employed to fabricate metal anti-corrosive coating on the surface of low-carbon steel by using drop-casting and thermosetting techniques. Moreover, Fourier transform infrared (FTIR) spectroscopy and thermogravimetric (TG) were used to analyze the structural changes during the curing process and thermal stability of the coating. The anti-corrosion performance and corrosion resistance mechanism were analyzed using electrochemical characterization, as well as static contact angle measurements and scanning electron microscopy-energy dispersive spectroscopy (SEM-EDS).

2. EXPERIMENTAL SECTION

2.1. Materials

4-(Phenylazo)phenol (95%), polyetheramine (D230, D400, D2000) (95%), paraformaldehyde (95%), toluene (99.9%), sodium hydroxide (99.0%), anhydrous sodium sulfate (99.0%), and sodium chloride (99.0%) were purchased from Kelong Chemical Reagents Corp., Chengdu, China. These materials were used as received.

2.2. Preparation of polyetheramine benzoxazine monomers

The synthesis process of benzoxazine monomers is illustrated in Scheme 1. In a three-necked round bottom flask, 100 mL of toluene was added as a reaction solvent and then, 3.03 mL (12.5 mmol) of polyetheramine D230 and 1.5 g (50 mmol) of paraformaldehyde were added. The mixture was stirred at room temperature and 4.955 g (25 mmol) of 4-(phenylazo)phenol was added into the completely dissolved mixture. Then, the temperature was increased to 110 °C and maintained for 12 h, followed by toluene removal under reduced pressure. The crude product was washed thrice using 2 mol/L NaOH solution and then washed with deionized water. Finally, the product was vacuum-dried at 50 °C for 24 h, resulting in a dark-red-colored viscous liquid (Bza-d230). Bza-d400 and Bza-d2000 were also synthesized using the same method by varying the polyetheramine grade.

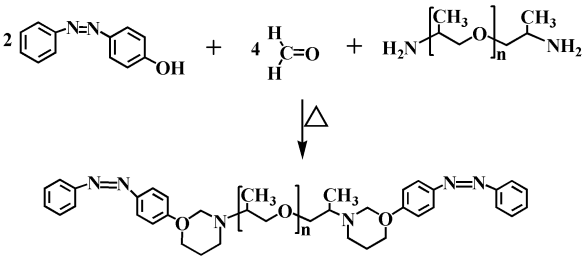

Schematic 1. The synthesis process of Bza monomer.

2.3. Preparation of PBa coatings on low-carbon steel

Low-carbon steel was used as a substrate for the coating preparation. First, the low-carbon steel substrate was ground with sandpaper to remove excess impurities from the surface. Then, it was placed in acetone solvent for ultrasonic washing for 20-30 minutes to further remove the surface impurities and engine oil for later use. The low-carbon steel with simple surface treatment was named as MS. The coatings were prepared by the following steps: In the case of Bza-d230, a viscous N,N-dimethylformamide (DMF) solution of Bza-d230 was prepared with a concentration of 100 g/L. Then, the solution was drop cast on the MS surface and the residual solvent was removed in a vacuum oven at 80 ^{o}C for 2 h. Finally, the coated MS substrates were cured at 200, 220, and 240 ^{o}C for 2 h, and the corresponding samples were marked as PBza-d230, PBza-d400, and PBza-d2000. The thickness of the coating was around 5 ± 0.1 μm.

2.4. Material characterization

2.4.1. Structural analysis

FTIR spectra were measured using a Nicolet 6700 FTIR analyzer. The solid sample was ground and an appropriate amount of solid powder was mixed with KBr using a mortar and pestle. Then, a KBr dropper was used to ensure uniform distribution and characterization. Moreover, proton nuclear magnetic resonance (^{1}H-NMR) spectra were recorded using a ^{1}H NMR spectrometer (Bruker AVANCE III HD 400) with $CDCl_3$ as a solvent and TMS as an internal standard.

2.4.2. Polymerization behavior

The dynamic polymerization reactions for polyetheramine-based benzoxazines were monitored using a PerkinElmer Diamond Differential Scanning Calorimeter under nitrogen, and the samples were scanned at a heating rate of 15 °C min^{-1}.

2.4.3. Thermal stability

Thermogravimetric analysis (TGA) was carried out using a TA Instrument Model 2050 with a heating rate of 10 °C/min under nitrogen flow at 40 mL/min.

2.4.4. Surface properties

DataPhysicsOCA25 contact angle instrument was used to measure the static contact angle of the coating. The needle-in test method was used with the test medium of distilled water and droplet volume of 3 μL. Five independently measured values were averaged out to obtain the contact angle of the coating.

2.4.5. Surface topography and adhesion measurement

The surface morphology of the coating was observed by scanning electron microscopy-energy dispersive spectroscopy (SEM-EDS). According to the GB/T 9286-1998 standard, the cross-cut test was used to evaluate the adhesion level of the anti-corrosion coating. First, parallel and equal cuts were placed on the sample coating according to the sample size. Then, vertical cuts were made and the number and spacing were adjusted to form a tic-tac-toe grid. During manual cutting, the force should be uniform and stable without trembling to ensure that the knife edge just penetrates the coating and does not touch the base material. One should note that large and uneven cuts can impact the test results. When the cutting was completed, the sample exhibited small squares of uniform size. The remaining debris was gently brushed off using a soft brush. Then, the surface conditions and coating adhesion were evaluated.

2.4.6. Corrosion characterization

The corrosion resistance was characterized by open circuit potential (E_{ocp}) *vs*. time curves, Tafel plots and electrochemical impedance spectroscopy (EIS) using an Aotulab PGSTAT302N. The samples were immersed in 3.5% sodium chloride solution for 10 minutes to attain a stable state before electrochemical characterization. Each test was repeated thrice to minimize the measurement error.

The Tafel plots were measured in the potential range of ± 500 mV (*vs*. Ag/AgCl) at the scan rate of 2 mV/s. The electrochemical workstation software was used to fit the Tafel curves and obtain I_{corr} and E_{corr} values. EIS was conducted under an AC signal amplitude of 10 mV in the frequency range of 100 kHz to 0.01 Hz.

3. RESULTS AND DISCUSSION

3.1. Structural characterization

Three di-functional benzoxazines were synthesized from 4-(phenylazo)phenol, polyetheramine (D230, D400, D2000), and paraformaldehyde, and the synthesis process is shown in Scheme 1. The chemical structure of the benzoxazines was confirmed by ^{1}H-NMR and FTIR spectra.

The ^{1}H-NMR spectra of polyetheramine-based benzoxazines are presented in Figure 1(a)-(c). It can be seen that the characteristic methylene proton signals of the oxazine ring appear at 4.01-4.11(Ar–CH_2–N) and 4.85-5.04 (O–CH_2–N) ppm, respectively[24]. The characteristic peak at 7.26 ppm can be ascribed to the proton peak of hydrogen in tritiated chloroform ($CDCl_3$). Also, the characteristic peak of hydrogen on the benzene ring is at 6.88-6.91 ppm. The chemical shifts of the characteristic peaks of hydrogen in the polyetheramine structure are: 1.07-1.20 (Ha, Hf), 3.15-3.39 (Hb, He), and 3.51-3.56 (Hc, Hd) ppm[25,26], indicating that polyetheramine is successfully grafted on the benzoxazine matrix.

The FTIR spectra of polyetheramine-based benzoxazines are presented in Figure 1(d). The characteristic absorption peaks at 2970-2976 cm^{-1} and 2863-2869 cm^{-1} can be assigned to the asymmetric stretching vibrations of C-H in methyl and methylene groups on polyether chains, respectively. The characteristic absorption peaks at 1670-1675 cm^{-1} and 1592-1599 cm^{-1} correspond to the benzene ring. The symmetric and asymmetric absorption vibrations of C-O-C on the oxazine ring are depicted by peaks at 1017 cm^{-1} and 1233-1245 cm^{-1}, respectively[24,27]. The characteristic peak at 1106 cm^{-1} is associated with the C-O-C asymmetric stretching of the polyether skeleton. The characteristic absorption peak of the oxazine ring is observed at 916-923 cm^{-1}. The FTIR and NMP results confirm that the desired product is successfully synthesized.

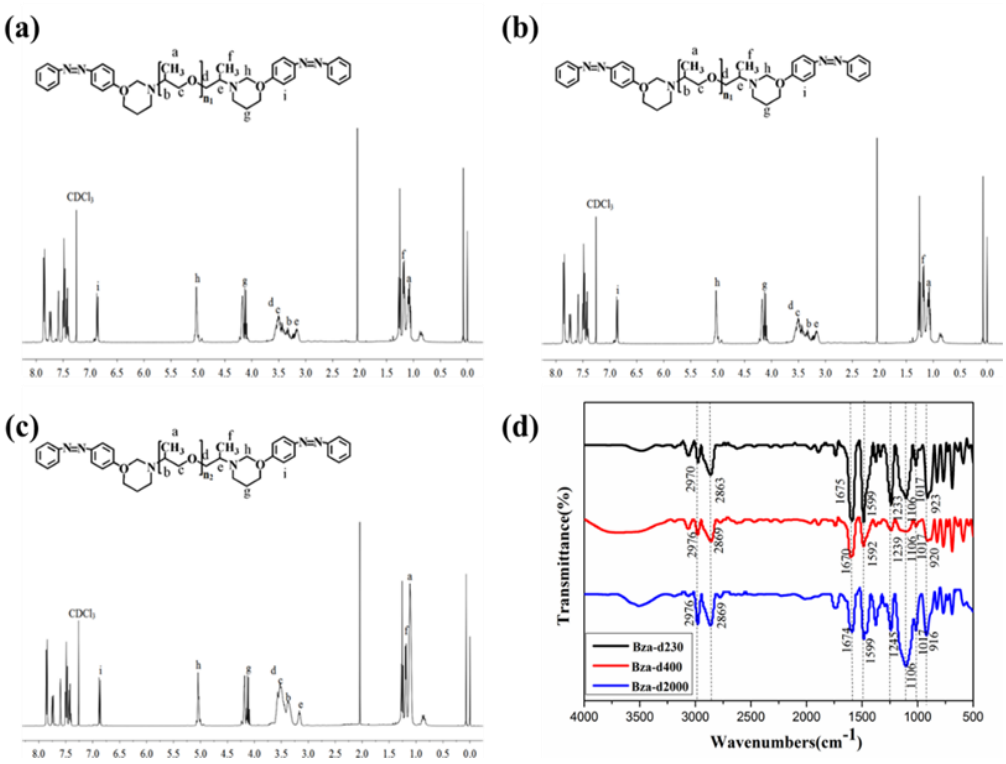

Figure 1. (a) ^{1}H NMR spectra of Bza-d230; (b) ^{1}H-NMR spectra of Bza-d400; (c) ^{1}H-NMR spectra of Bza-d2000; (d) FTIR spectra of polyetheramine-based benzoxazines.

3.2. Structural changes during polymerization

The FTIR spectra of the polyetheramine-based benzoxazines and corresponding products after heating at different temperatures in air for the same time are shown in Figures 2, 3, and 4, with untreated polyetheramine-based benzoxazines as a control. Significant changes are observed in the intensity of characteristic absorption peaks at 916, 918, 925, and 1233-1276 cm^{-1}, corresponding to the oxazine ring structure. The oxazine ring structure almost disappears after curing at 200 ℃, 220 ℃, and 240 ℃ for 2 h, indicating that the degree of oxazine ring-opening polymerization is completed. Correspondingly, the intensity of absorption peaks at 1476, 1373, 822, and 767 cm^{-1} also gradually weakens or even disappears, indicating that the number of substituents on the benzene ring increase

during the curing process. On the other hand, the intensity of absorption peak at 3457 cm^{-1}, corresponding to phenolic hydroxyl, gradually increases because the ring-opening process generates a new phenolic hydroxyl group. Moreover, the intermediate product-Schiff base (N=CH) is produced during the ring-opening process, as depicted by a characteristic peak at 1635 cm^{-1}[28-30].

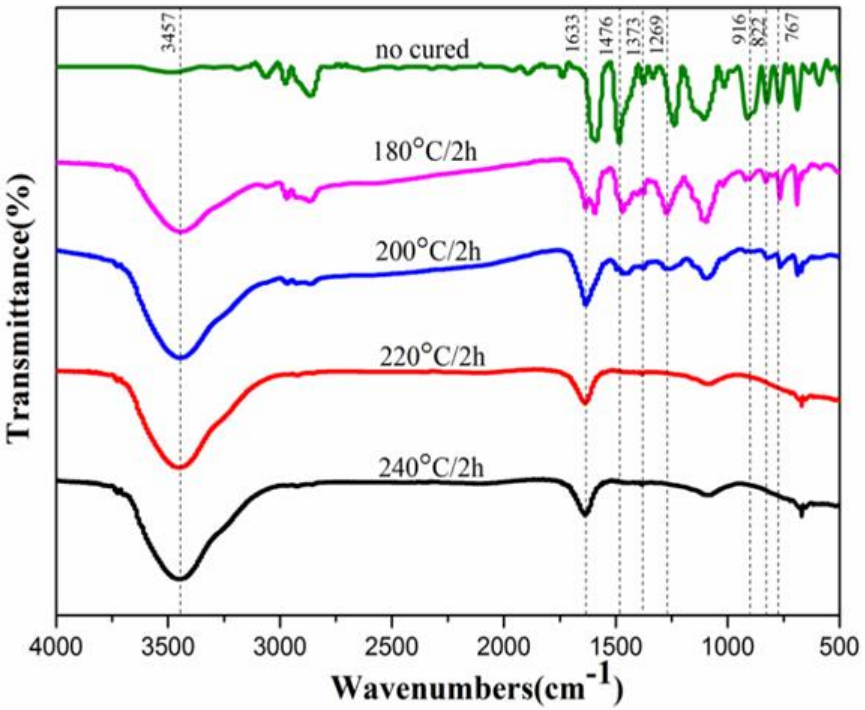

Figure 2. FTIR spectra of Bza-d230 after curing at different temperatures for 2 h.

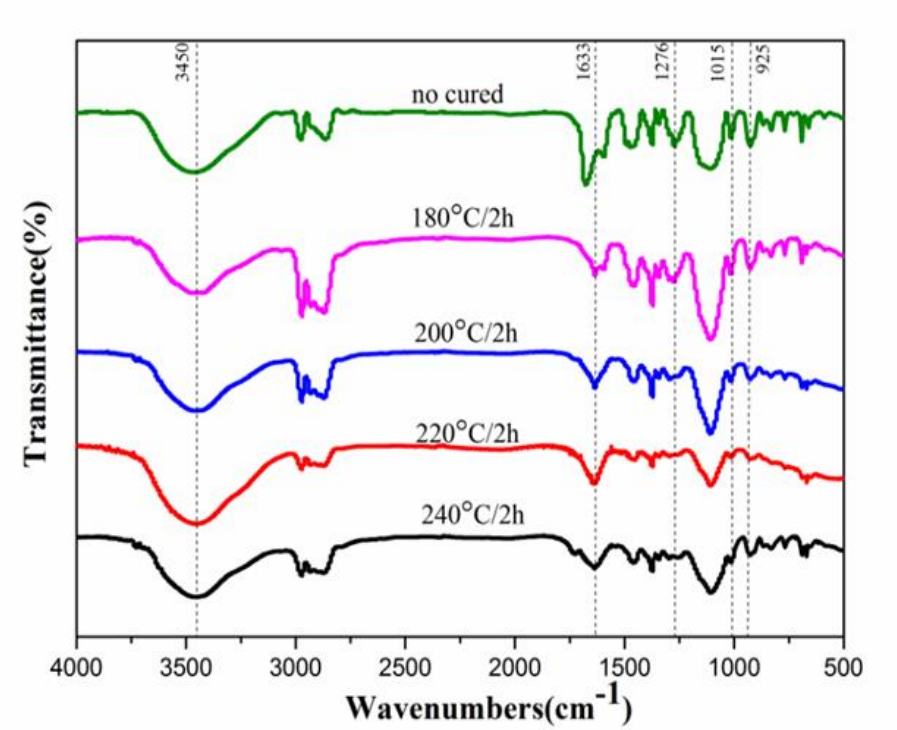

Figure 3. FTIR spectra of Bza-d400 after curing at different temperatures for 2 h.

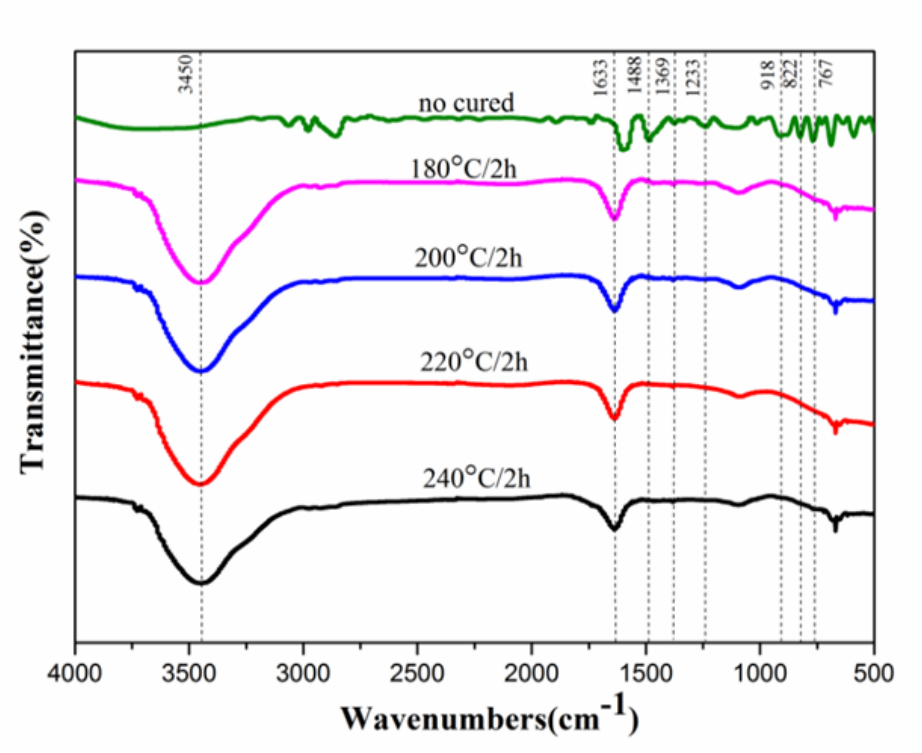

Figure 4. FTIR spectra of Bza-d2000 after curing at different temperatures for 2 h. *Surface properties*

Coatings were prepared by adding different polyetheramine-based benzoxazines, followed by thermal curing. The coatings were labeled as PBza-d230, PBza-d400 and PBza-d2000. The contact angle was measured for the MS and as-prepared polybenzoxazine coatings to probe their hydrophobicity, as exhibited in Figure 5. In general, a large contact angle corresponds to high hydrophobicity[31,32].

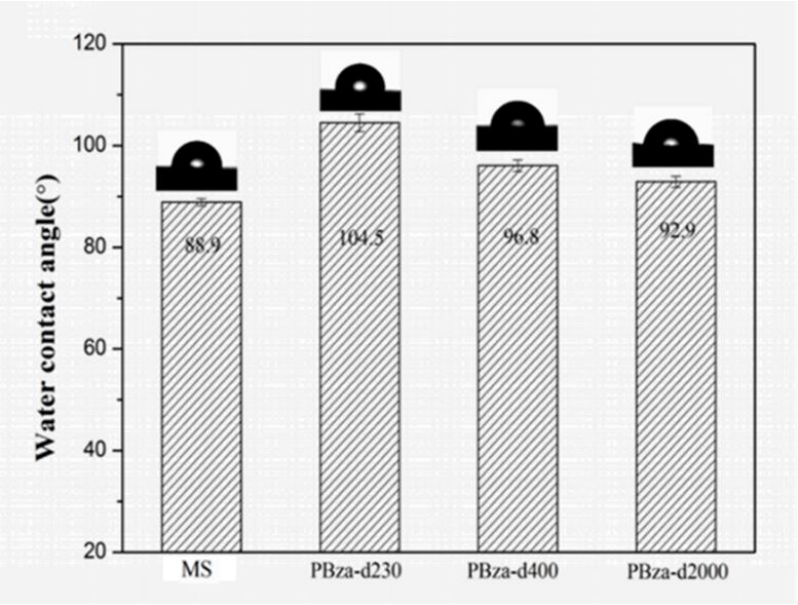

Figure 5. The profiles of water droplets of MS, PBza-d230, PBza-d400, and PBza-d2000.

The contact angles of the PBza-d230, PBza-d400, and PBza-d2000 coatings are found to be 104.5, 96.8, and 92.9°, respectively, all of which are slightly higher than the contact angle of pristine MS (88.9°). Obviously, the hydrophobicity of coatings is significantly improved because the low surface energy of PBa can provide water insulation to the low-carbon steel substrate.

In addition, polyether amine contains polyether segments, which are hydrophilic groups and lead to certain water absorption. Therefore, the contact angle decreases with the increase in polyether content. In addition, the film-forming ability of the as-prepared material was investigated by SEM. As shown in Figure 6, the as-prepared polybenzoxazine coatings possess a uniform surface without obvious defects, indicating excellent film-forming ability and ductility. One should note that traditional benzoxazines are mostly solid powders, which are difficult to process into thin films without solvents, and exhibit high sensitivity to solvents during dissolution. The as-prepared polyetheramino-based benzoxazines are liquid at room temperature and can be fully dissolved in common solvents, such as DMF and dichloromethane, improving the ductility and flexibility of polybenzoxazine coatings.

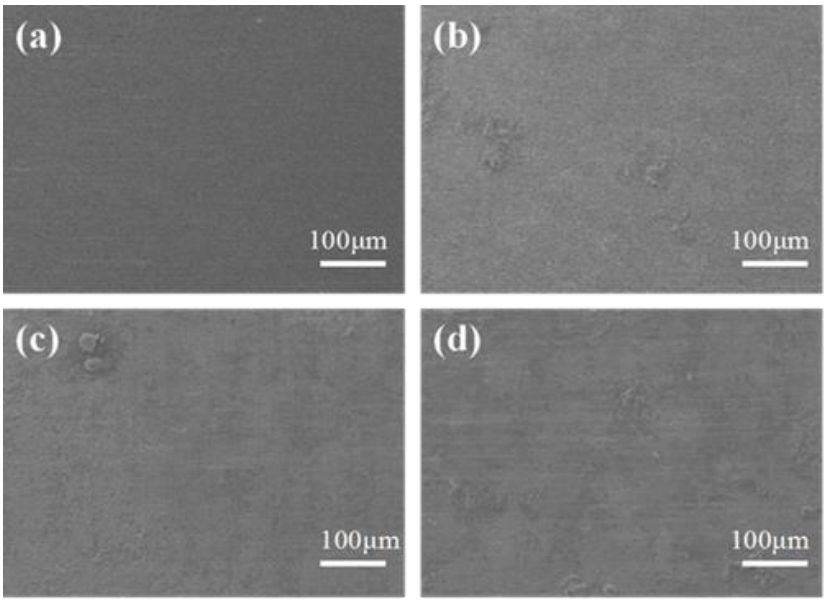

Figure 6. SEM images of (a) MS, (b) PBza-d230, (c) PBza-d400, and (d) PBza-d2000.

The excellent adhesion between the coating and substrate is closely related to the corrosion resistance of the coating. Herein, the cross-hatch test method was used to investigate the adhesion of three polybenzoxazine coatings on the surface of mild steel.

Figure 7 shows the SEM images of samples after the adhesion test. The results of PBza-d230, PBza-d400, and PBza-d2000 coatings were evaluated according to the GB/T 9286-1998 standard. A small amount of peeling is observed at the scratch edges of the PBza-d230 and PBza-d400 coatings, whereas the scratch edges of the PBza-d2000 coating are relatively flat and smooth without any peeling. These results confirm that the adhesion of PBza-d230 and PBza-d400 coatings is similar to 3B (the adhesion evaluation standard, shown in Figure 7(e)), whereas the adhesion of PBza-d2000 coating is close to category 1B. For 3B category in the adhesion test, part or all of the coating fell off in pieces

along the cutting edge, or on different parts of the grid. The proportion of fallen off coating was more than 15% and less than 35%. Conversely, for 1B category, there was a little flake separation at the intersection of the cuts, but the cross-cut area was clearly not greater than 5%. It is worth mentioning that the incorporation of flexible segments improves the adhesion of PBza. In general, the polymers possess fewer flexible segments with low molecular weight, high rigidity, and brittleness. Therefore, the adhesion between metallic substrate and coating is quite low.

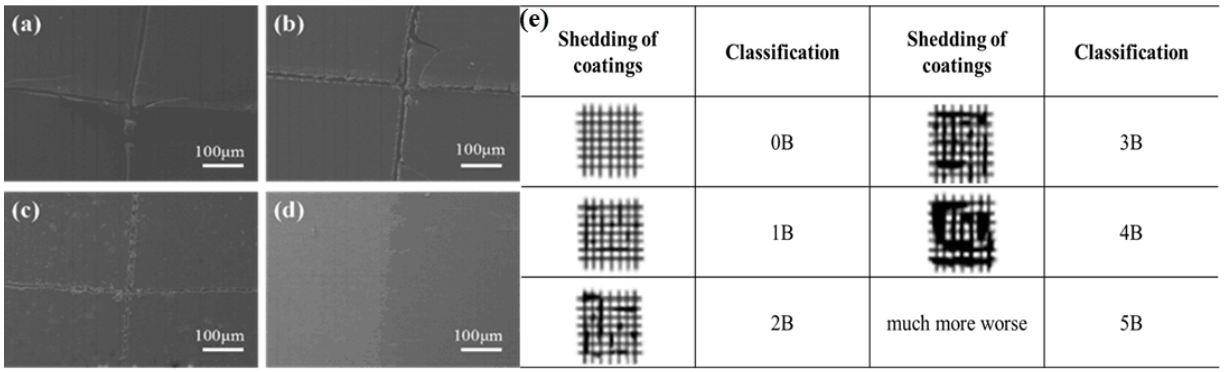

Figure 7. SEM images of (a) MS, (b) PBza-d230, (c) PBza-d400 and (d) PBza-d2000. (e) Adhesion evaluation standard.

3.4. Electrochemical characterization

The as-prepared coatings were electrochemically tested in 3.5 wt.% NaCl solution to investigate the corrosion behavior. In order to ensure the stability of the system, the samples were immersed in 3.5 wt.% aqueous NaCl solution for approximately 2 minutes prior to the OCP measurements. Figure 8 shows the E_{ocp} *vs*. time curves of the as-prepared coatings.

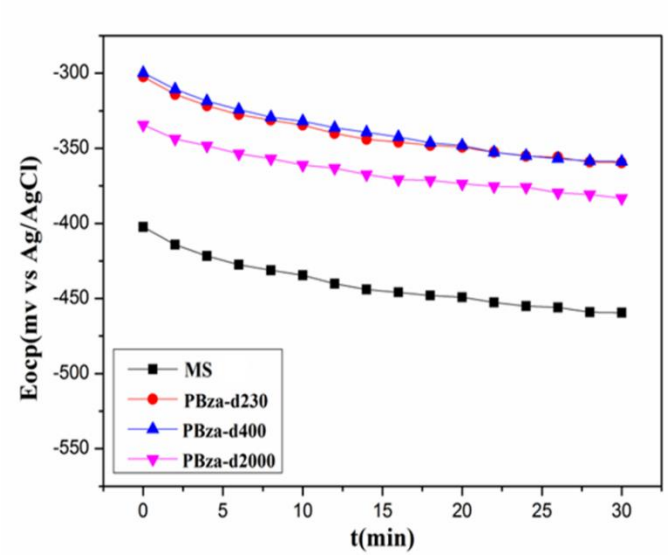

Figure 8. The E_{ocp} *vs*. time curves of as-prepared coatings in aqueous 3.5 wt.% NaCl solution.

As shown in Figure 8, the initial E_{ocp} value of the as-received MS is -402 mV (*vs*. Ag/AgCl), which decreases to -459 mV (*vs*. Ag/AgCl) after being immersed for 30 minutes. However, the initial E_{ocp} values of PBza-d230, PBza-d400 and PBza-d2000 are −302, −299, and −334 mV (*vs*. Ag/AgCl), respectively, rendering better shielding than the as-received MS after being immersed in NaCl solution for 30 minutes. The high E_{ocp} values correspond to the high corrosion resistance of the as-prepared coatings[33]. The PBza-d400 coating exhibits the largest E_{ocp} and best shielding ability to the corrosive media. It may be related to the high content of polyether segments in PBza-d400, leading to a large free volume between structural units. Hence, the hydroxyl groups (-OH) do not alter the spacing, and increase the cross-linking density of the polymers.

Table 1. The results of electrochemical measurements for MS and as-prepared coatings.

Sample	E_{corr} (mV)	I_{corr} / (A·cm^{-2})	R_c / (mm·a^{-1})	E / %
MS	-402	5.24×10^{-5}	6.09×10^{-1}	—
PBza-d230	-302	5.83×10^{-7}	6.78×10^{-3}	98.89
PBza-d400	-299	3.47×10^{-7}	4.03×10^{-3}	99.34
PBza-d2000	-334	7.43×10^{-7}	8.64×10^{-3}	98.58

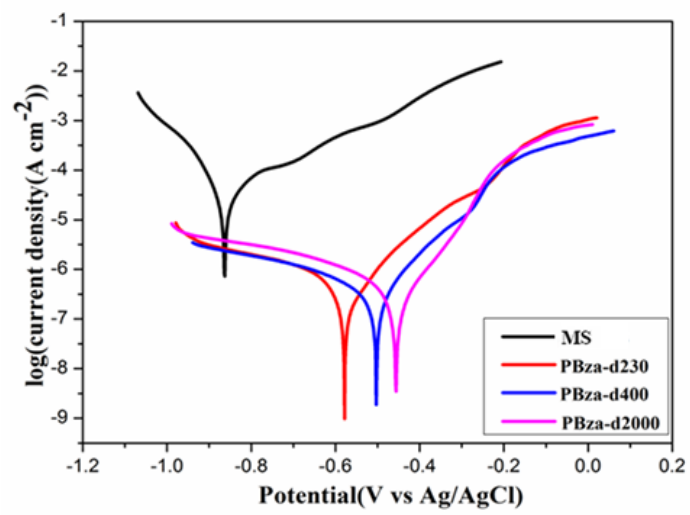

Figure 9. Tafel curves of MS and as-prepared coatings in aqueous 3.5 wt.% NaCl solution.

The corrosion potential (E_{corr}) and corrosion current density (I_{corr}) of different samples were obtained by the Tafel extrapolation method[34,35]. The corrosion rate can be given as:

$$R_c = \frac{KM_m I_{corr}}{n\rho m}$$

where the constant value of corrosion rate (K) is 3268.5 mol/(A·a), the value of equivalent weight (M_m) is 55.85 g/mol, *n* refers to the number of charge transfer, and the density of low-carbon steel is usually taken as 7.85 g/cm^3. The protection rate of the coating can be given as:

$$E=\frac{I_{corr}-I_{corr(c)}}{I_{corr}}$$

where I_{corr} and $I_{corr\,(c)}$ refer to the corrosion current values in the absence and presence of the coatings, respectively. The corrosion parameters of the as-prepared coatings are summarized in Table 1.

Figure 9 presents the Tafel plots of MS and as-prepared coatings. The I_{corr} of different samples was obtained by the Tafel extrapolation method[36,37]. A lower polarization current of the coating corresponds to better corrosion resistance[38]. Compared with the as-received MS, the corrosion potential of the polybenzoxazine-coated MS is shifted to a positive value, and both anodic and cathodic currents decrease, indicating the high corrosion resistance of PBza-d230, PBza-d400, and PBza-d2000. The Tafel curves of the polybenzoxazine coatings exhibit lower I_{corr} values (5.83×10^{-7}, 3.47×10^{-7}, 7.43×10^{-7}) than the as-received MS (5.24×10^{-5}), indicating a reduction of over two orders of magnitude. In addition, compared with the as-received MS (6.09×10^{-1} mm·a^{-1}), the corrosion rates of the PBza-d230, PBza-d400 and PBza-d2000 coatings also decrease to 6.78×10^{-3} mm·a^{-1}, 4.03×10^{-3} mm·a^{-1}, and 8.64×10^{-3} mm·a^{-1}, respectively, showing a remarkable protection efficiency of >98%. Hence, polybenzoxazine coating can effectively inhibit the infiltration of corrosive media and enhance the corrosion resistance of the low-carbon steel.

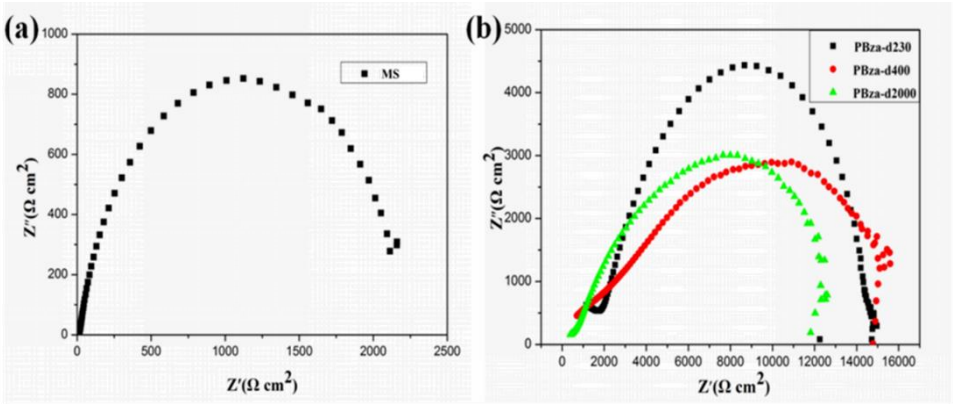

Figure 10. The Nyquist curves of as-received MS and as-prepared coatings.

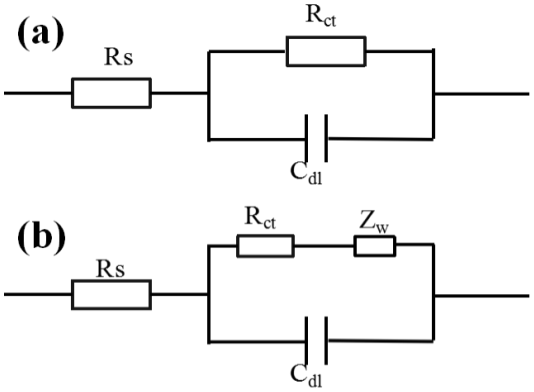

Figure 11. The equivalent circuit model for the (a) as-received MS and (b) polybenzoxazine coatings.

The electrochemical behavior of pristine MS and benzoxazine coatings was also investigated by room-temperature EIS. Figure 10 presents Nyquist plots of MS and as-prepared coatings. The size of capacitive arc is directly related to the corrosion resistance of the coating[39]. It can be seen from the Nyquist curve that polybenzoxazine coatings exhibit only one capacitive arc, indicating that all polybenzoxazine coatings possess only one chemical interface. Hence, the coating has a good shielding effect on the corrosive medium and the corrosive medium cannot penetrate to the surface of substrate to chemically react and corrode the substrate.

Compared with the as-received MS, the capacitive resistance arc of the polybenzoxazine coatings is significantly increased and the PBza-d400 coating exhibits the largest capacitive resistance arc. Herein, an equivalent electric circuit model is obtained by fitting the EIS results, as shown in Figure 11, where Rs represents solution resistance, constant phase element (C_{dl}) depicts the electric double-layer capacitance at metal/liquid interface and R_{ct} corresponds to the polymer resistance (metal-polymer interface resistance or polymer solution resistance)[40,41]. The R_{ct} can be used as a measure of the corrosion resistance, where a high R_{ct} value indicates high resistance[41].

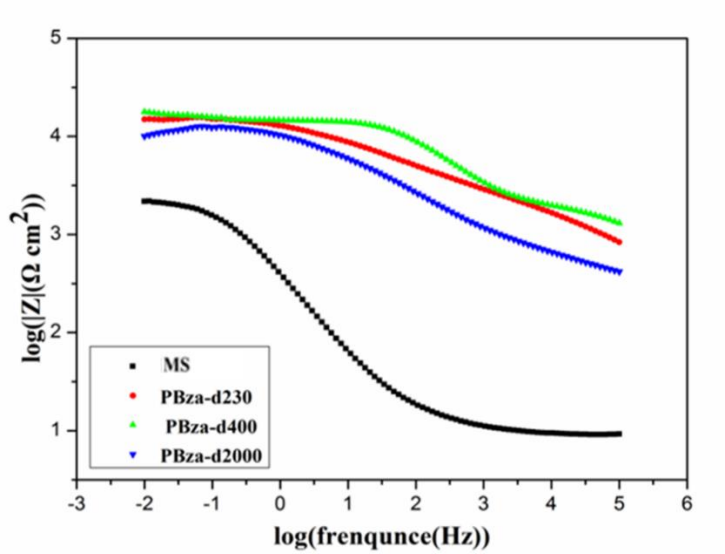

Figure 12. The Bode plots of as-received MS and as-prepared coating in aqueous 3.5 wt.% NaCl solution.

Figure 12 presents the Bode plots of different samples in aqueous 3.5 wt.% NaCl solution. In the Bode graphs, the high-frequency area represents the corrosion phenomenon that occurs in the medium, whereas the low-frequency area represents the anti-corrosion performance of the coating. Also, the impedance modulus |Z| value in the low-frequency region represents the corrosion resistance of the coating. The capacitance and resistance of the coating determine the value of |Z|. The value of |Z| decreases with higher capacitance and lower resistance[42]. As shown in Figure 15, compared with the as-received MS, the Bode impedance modulus of the as-prepared coatings is significantly increased. The |Z| value of the as-received MS at 0.01 Hz is 2.19×10^3 Ω·cm^2, while the |Z| values of PBza-d230, PBza-d400 and PBza-d2000 at 0.01 Hz are 1.48×10^4 Ω·cm^2, 1.78×10^4 Ω·cm^2, and $1.0 \times$

10^4 Ω·cm^2, respectively. Compared with the as-received MS, it is an order of magnitude higher and corresponds to excellent corrosion resistance. Herein, the PBza-d400 coating exhibits the largest |Z| value at 0.01 Hz, corresponding to the optimal corrosion resistance.

In other words, PBza-d400 coating exhibits better shielding and corrosion resistance than the PBza-d230 and PBza-d2000 coatings, which can be ascribed to its densely cross-linked structure and hydrogen-bonded network, inhibiting the access of corrosive medium to the steel substrate.

3.5. Corrosion surface

Figures 13, 14, and 15 show the corrosion-surface morphology of PBza-d230, PBza-d400 and PBza-d2000 after being immersed in 3.5 wt.% NaCl solution for 24 h, respectively. The substrate surface of the three coatings exhibits different degrees of corrosion. The EDS analysis shows that the weight percentages of Fe, O, Na, and Cl on the surface of PBza-d230-coated steel are 91.44%, 6.70%, 1.05%, and 0.81%, respectively. Similarly, the weight percentages of Fe, O, Na, and Cl on the surface of PBza-d400-coated steel are 96.28%, 2.50%, 0.64%, and 0.58%, whereas the weight percentages of Fe, O, Na, and Cl on the surface of PBza-d2000-coated steel are 93.72%, 4.73%, 0.93%, and 0.62%, respectively. The presence of Na and Cl confirms that the surface of low-carbon steel is corroded in 3.5 wt.% NaCl solution, whereas the higher amounts of O and Cl indicate more severe corrosion reaction[43]. Therefore, EDS analysis confirms that the PBza-d400-coated steel has the minimum amounts of O and Cl elements, corresponding to the optimal corrosion resistance.

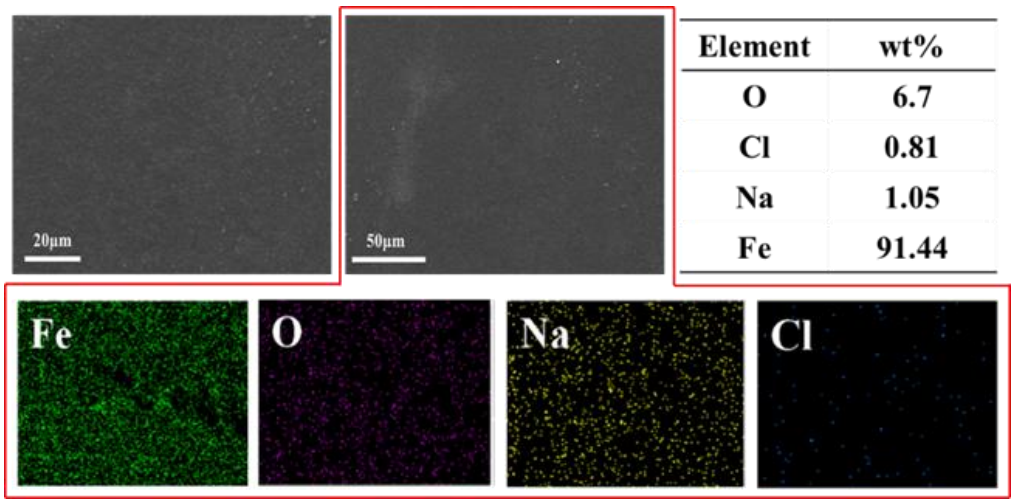

Figure 13. SEM images, EDS maps, and contents of different elements from the corroded regions of PBza-d230-coated steel.

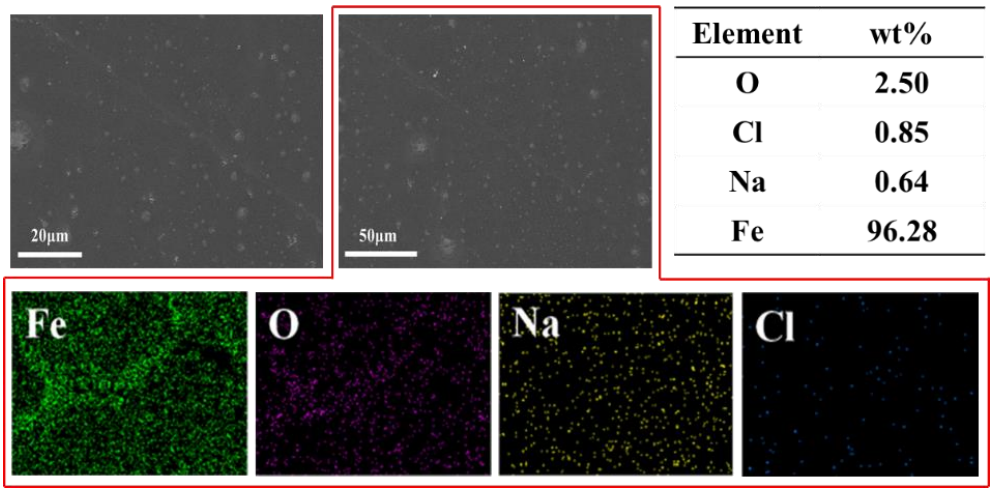

Element	wt%
O	2.50
Cl	0.85
Na	0.64
Fe	96.28

Figure 14. SEM images, EDS maps, and contents of different elements from the corroded regions of PBza-d400-coated steel.

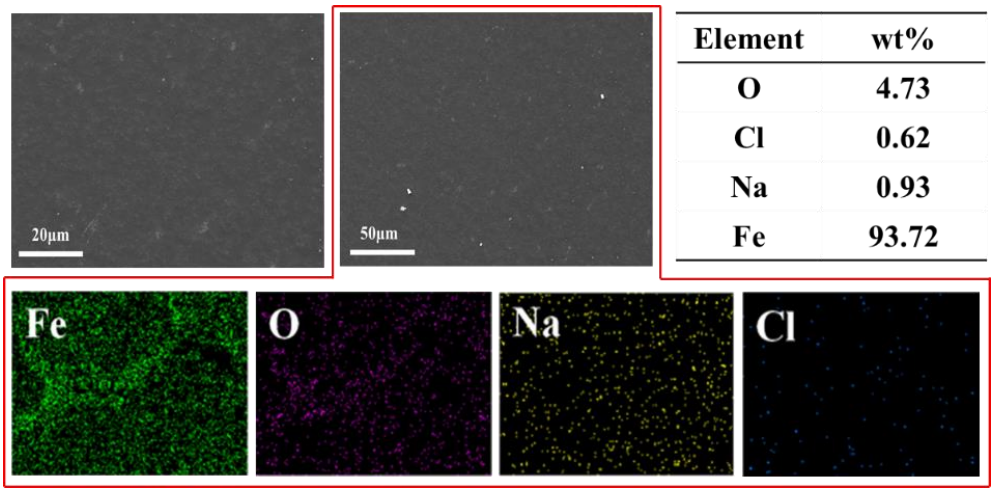

Element	wt%
O	4.73
Cl	0.62
Na	0.93
Fe	93.72

Figure 15. SEM images, EDS maps, and contents of different elements from the corroded regions of PBza-d2000-coated steel.

4. CONCLUSIONS

In summary, based on the flexible molecular design of benzoxazines, three polyetheramine benzoxazines were successfully synthesized using the solution method, followed by thermal curing. These coatings overcome the shortcomings of the traditional polybenzoxazine resin coatings, such as inferior film formation and high brittleness. The corrosion protection ability of polybenzoxazine coatings was investigated by open circuit potential measurement, potentiodynamic polarization curves, and EIS. The results revealed that these coatings inhibit the access of corrosive medium to the metal surface and enhance the corrosion resistance. These coatings hold promising application prospects due to their simple preparation, easy storage, and excellent anti-corrosive characteristics.

ACKNOWLEDGEMENT
This work was funded by Science and Technology Program of Sichuan (grant number 2021YFH0031, 2022YFG0270, and 2022YFG0113).

INSTITUTIONAL REVIEW BOARD STATEMENT
Not applicable.

INFORMED CONSENT STATEMENT
Not applicable.

DATA AVAILABILITY STATEMENT
Not applicable.

CONFLICTS OF INTEREST
The authors declare no conflict of interest.

References

1. S. Kumar, H. Vashisht and L. O. Olasunkanmi, *Sci. Rep.,* 6(2016)2045.
2. X. Lu, Y. Liu and C. L. Zhou, *RSC Adv*., 6(2016)5805.
3. J. Huang, L. Chang, D. Xu, X. Lu, Z. Xin and C. L. Zhou, *Prog. Org. Coat*., 136(2019)105191.
4. X. F. Zheng, Y. Q. Chen and J. M. Hu, *Corros Sci*., 166(2020)108452.
5. V. Singh, S. Kumar and D. J. Ratha, *J. Tribol*., 142(2020)101401.
6. D. G. Kumar, N. Shova, S. Sanjay, K. Nabin and P. Y. Amar, *Prog. Org. Coat*., 152(2021)106127.
7. S. S. Jia, X. H. Lu, S. Luo, Y.Qing, N. Yan and Y. Q. Wu, *Chem. Eng. J*., 348(2018)212.
8. F. Á. María, V. Francisco, B. Asunción, G. G. Yaiza and G. Beatriz, *J. Electrochem. Soc*., 167(2020) 0016.
9. B. Ramezanzadeh, G. Bahlakeh and M. Ramezanzadeh, *Corros. Sci*., 137(2018)111.
10. S. L. Li, C. X. Zhao, Y. N. Wang, H. Li and Y. T. Li, *J. Mater. Sci*., 53(2018) 7344.
11. Y. C. Zhou, P. Z. Li and Z. F. Xu, *Polym. Compos*., 35(2014)617.
12. Q. Li and Z. Xin, *Langmuir*., 27(2011)8365.
13. V. N. Sokolik, S. F. Gizatullin, I. M. Raigorodskii, and V. M. Kopylov, *Polym. Sci. Ser*. D., 10(2017)123.
14. W. Z. Zhang, N. Jiang and T. T. Zhang, *J. Elastomers Plast*.,53(2021)0095.
15. Y. T. Zhang, X. Y. Liu, G. Z. Zhan, Q. X. Zhuang, R. H. Zhang and J. Qian, *Eur. Polym. J*., 119(2019)477.
16. G. A. Phalak, D. M. Patil and S. T. Mhaske, *Eur. Polym. J*., 88(2017)93.
17. C. Aydogan, B. Kiskan, S. O. Hacioglu, L. Toppare and Y. Yagci, *RSC Adv*., 4(2014)27545.
18. S. C. Lin, C. S. Wu, J. M. Yeh andY. L. Liu, *Polym. Chem*., 5(2014)4235.
19. E. B. Caldona, A. C. Leon, B. B. Pajarito and R. C. Advincula, *Appl. Surf. Sci*., 422(2017)162.
20. A. Renaud, L. Bonnaud, L. Duma, T. Zhang and Y. Paint, *Eur. Polym. J.,* 109(2018)460.
21. X. Lu, Y. Liu, C. L. Zhou, W. F. Zhang and Z. Xin, *RSC Adv*., 6(2016)5805.
22. J. Huang, L. Chang, D. Xu, X. Lu, Z. Xin and C. L. Zhou, et al. *Prog. Org. Coat*., 136(2019)0300.
23. Y. T. Zhang, X. Y. Liu, G. Z. Zhan, Q. B. Zhuang, R. H. Zhang and J. Qian, *Eur. Polym. J.,* 119(2019)477.
24. Y. F. Liu, J. B. Huang, X. H. Su, M. Han, H. Li, M, T, Run, H. Z, Song and Y. G. Wu, *React. Funct. Polym.*, 102(2016)62.
25. S. N. Zhang, Y. Q. Peng, W. H. Xue, S. S. Shen, C. Y. Li, Z. Y. Li and Y. F. Liu, *Polym*., 166(2019)169.

26. G. S. Lu, H. Y. Yang, H. C. Zhen, C. Y. Li, S. S. Shen, Y. F. Liu and M. T. Run, *Int. J. Polym. Anal. Charact*., 25(2020)397.
27. J. Dunkers, H. Ishida, *Spectrochim. Acta, Part* A., 51(1995)1061.
28. H. J. Kim, Z. Brunovska, H. Ishida, *Polymer*, 40(1998)1815.
29. D. J. Allen, H. Ishida, *Polymer*, 48(2008)6763.
30. B. S. Shyan, I. Hatsuo, *J. Appl. Polym. Sci*., 61(1996)1595.
31. D. Q. Zhu, W. J. V. Ooij, *Electrochimica Acta*., 49(2004)1113.
32. J. M. Yeh, C. J. Weng and W. J. Liao, *Surf. Coat. Technol*., 201(2006)1788.
33. C. L. Zhou, X. Lu, Z. Xin and J. Liu, *Corros. Sci*., 70(2013)145.
34. W. G. Ji, J. M. Hu and J. Q. Zhang, *Corros. Sci*., 48(2008)3731.
35. P. Wang, D. Zhang and Z. Lu. *Corros. Sci*., 90(2015)23.
36. V. Annibaldi, A. D. Rooney and C. B. Breslin, *Corros. Sci*., 59(2012)179.
37. S. H. Mosavat, M. H. Shariat and M. E. Bahrololoom. *Corros. Sci*., 59(2012)81.
38. F. Z. Zhang, L. L. Zhao and H. Y. Chen, *Angew. Chem. Int. Ed*., 47(2008)2466.
39. F. Ansari, R. Naderi and C. Dehghanian, *RSC Adv.*, 5(2015)706.
40. S. Suttiruk, A. A. Krisada and T. Kusuma, *Adv. Mater. Interfaces*., 7(2020)2196.
41. A. A. ElShami, S. Bonnet and M. H. Makhlouf, *Pigm. Resin Technol*., 49(2020)501.
42. S. C. Di, Y. P. Guo and H. W. Lv, *Ceram. Int.*, 41(2015)6178.
43. S. L. Li, C. X. Zhao, H. L. Gou, *Int. J. Electrochem. Sci.*, 13(2018)2661.